Catalytic Twist-Spun Yarns of Nitrogen-Doped Carbon Nanotubes

Xavier Lepró, Raquel Ovalle-Robles, Márcio D. Lima, Ana Laura Elías, Mauricio Terrones, and Ray H. Baughman*

The treatment of free-standing sheets of multiwalled carbon nanotubes (MWNTs) with a NH_3/He plasma results in self-supporting sheets of aligned N-doped MWNTs (CN_x). These CN_x sheets can be easily twist spun in the solid state to provide strong CN_x yarns that are knottable, weavable, and sewable. The CN_x yarns exhibit tunable catalytic activity for electrochemically driven oxygen reduction reactions (ORR), as well as specific capacitances (up to 39 $F \cdot g^{-1}$) that are 2.6 times higher than for the parent MWNTs. Due to a high degree of nanotube alignment, the CN_x yarns exhibit specific strengths (451 ± 61 $MPa \cdot cm^3 \cdot g^{-1}$) that are three times larger than observed for hybrid CN_x/MWNT biscrolled yarns containing 70 wt.% CN_x in the form of a powder. This difference in mechanical strength arises from substantial differences in yarn morphology, revealed by electron microscopy imaging of yarn cross-sections, as well as the absence of a significant strength contribution from CN_x nanotubes in the biscrolled yarns. Finally, the chemical nature and abundance of the incorporated nitrogen within the CN_x nanotubes is studied as function of plasma exposure and annealing processes using X-ray photoelectron spectroscopy and correlated with catalytic activity.

1. Introduction

Carbon nanotubes (CNTs) exhibit high specific strengths and combination of properties that make them attractive for fabrication of multifunctional yarns and fibers.[1–3] Traditional routes for making carbon nanotube fibers involve solution or melt-based spinning of unoriented nanotubes that are dispersed in polymer-containing liquid or melt.[4] While some of these methods can be applied to various derivitized and substitutionally doped nanotubes, low accessible degrees of nanotube alignment, degradation of nanotube length during nanotube dispersion, and low nanotube concentrations can severely limit mechanical properties and electronic transport.[5,6] Additionally, the presence of a polymer matrix can restrict fiber multifunctional performance for such applications as for catalysis and electron field emission.[7–9]

Two main methods have been developed for the dry-state fabrication of aligned carbon nanotube yarns. The first one involves synthesis of CNTs in the gas phase using a floating catalyst method, collection of these largely unoriented nanotubes as an aerogel phase, and yarn draw from the aerogel.[10] Yarn stretch and densification by twist insertion or using surface tension effects can result in partially oriented yarns having attractive mechanical properties.[11] The second method involves the use of tightly controlled synthesis conditions to provide the special topologies needed to make CNT forests that are drawable into sheets or yarns.[5,6,12–16] From the edges of these special forests, aerogel-sheets of highly aligned CNTs can be easily drawn and eventually transformed into pure-CNT yarns by twist insertion using spinning methods like those used to make wool yarns.

The relative chemical inertness of yarns made of undoped CNTs limits their use for catalysis. However, recent research has demonstrated that N-doped CNTs (CN_x) have attractive catalytic properties for the oxygen reduction reaction (ORR),[17–20] which may become important for decreasing the costs of fuel cells and metal-air batteries by eliminating the need for expensive noble metals.[21] More specifically, weavable yarns made of CN_x could find applications in the medium term as woven textile electrodes for fuel cells and metal–air batteries.

Direct spinning of doped CNTs from forests of nitrogen-doped CNT forests has not been reported, which is not surprising since the usual synthesis conditions[22–28] for producing doped forests can interfere with the narrow set of conditions needed to provide forest "drawability". One way to obtain CN_x-containing yarns that are highly catalytic is to incorporate CN_x nanotubes as a guest powder in the spirals of a host carbon nanotube yarn using the newly invented "biscrolling" technology.[21] However, while biscrolled yarns can be weavable,

X. Lepró, Dr. R. Ovalle-Robles, Dr. M. D. Lima, Prof. R. H. Baughman
The Alan G. MacDiarmid NanoTech Institute
The University of Texas at Dallas
Richardson, TX 75083, USA
E-mail: xn.lepro@gmail.com
Dr. A. Laura Elías, Prof. M. Terrones
Department of Physics
Department of Materials Science and Engineering and Materials Research Institute
The Pennsylvania State University
104 Davey Lab., University Park, PA 16802, USA
Prof. M. Terrones
Exotic Nanocarbon Research Center
Shinshu University
Wakasato 4-17-1, Nagano 380-8553, Japan

DOI: 10.1002/adfm.201102114

knittable, sewable, and washable, the presence of the CN_x nanotube powder decreases yarn mechanical strength.

Post-synthesis doping is an alternative route to N-dope CNTs, which we will explore as a method for fabricating high strength, catalytic yarns containing only nitrogen doped nanotubes. Generic approaches consist in exposing the CNTs to highly reactive species of the desired dopant either aided by the use of high temperatures (1250–1350 °C),[29,30] ion implantation[31,32] or plasma.[33] Here, we demonstrate that treatment on a free-standing CNT sheet stack with a NH_3/He plasma results in free-standing sheets of aligned CN_x, which can be twist spun into strong yarns that are catalytic for electrochemically driven ORR. The effects of plasma treatment time and thermal annealing on catalytic activity were investigated. The catalytic performance of this new type of catalytic yarn was compared with that for biscrolled yarns prepared using as guest CN_x doped during nanotube synthesis (s-CN_x). The influence of the method used for yarn preparation on the yarn-morphology and the effects of this morphology on yarn mechanical properties were also analyzed.

2. Results and Discussion

The carbon nanotube sheets used in the present work were drawn from ~350 μm high forests comprising multiwalled carbon nanotubes (MWNTs) that have an outer diameter of ~9 nm, contain ~6 walls, and form large bundles.[21] Aligned stacks of N-doped MWNT (CN_x) sheets were prepared by exposing free-standing MWNT sheets to a NH_3/He plasma (using a 100 W RF source, 0.9 vol.% NH_3 and 900 mtorr total pressure). Plasma treatment times of up to 20 minutes were used; longer times were avoided because the mechanical integrity of the MWNT sheets began to degrade due to excessive CNT etching. Interestingly, when the plasma gas does not contain NH_3, the pure He plasma highly degrades the structural integrity of MWNT sheets in much shorter time (5 minutes) and the nanotube sheets are completely etched away in less than 10 minutes of plasma exposure.

Despite the harsh conditions that the NH_3/He plasma treatment provides, we found that 10 minutes of plasma treatment decreased the areal density ($\mu g \cdot cm^{-2}$) of the MWNT sheets by only 17%. This result was obtained by comparing the sheet absorbance at λ = 550 nm before and after plasma treatment. Morphology studies on the plasma treated MWNT sheets using scanning and transmission electron microscopy (SEM Zeiss Supra 40 and TEM JEOL 2100) indicate that the overall preferential alignment of CNTs is not noticeable changed; nevertheless changes in the surface of the CNTs were indeed observed. TEM images of tubes before and after the plasma treatment (**Figures 1**A–B, respectively) show the presence of amorphous-like material deposited on the outermost walls of the tubes as an apparent result of partial plasma etching. Moreover, micro-Raman spectra measurements (using a non-polarized laser at λ = 514 nm) (Figure 1C) show that loss of intrashell order increases with increasing plasma exposure times. D and G-band positions, their full width at half maximum (FWHM) and integrated intensities were obtained by applying mixed Gaussian–Lorentzian curve fitting to representative Raman spectra for each sample. Results were obtained by averaging measurements for at least three different areas for each plasma exposed and unexposed sheet. The ratio between the integrated intensity of the ~1350 cm^{-1} D-band to that for the

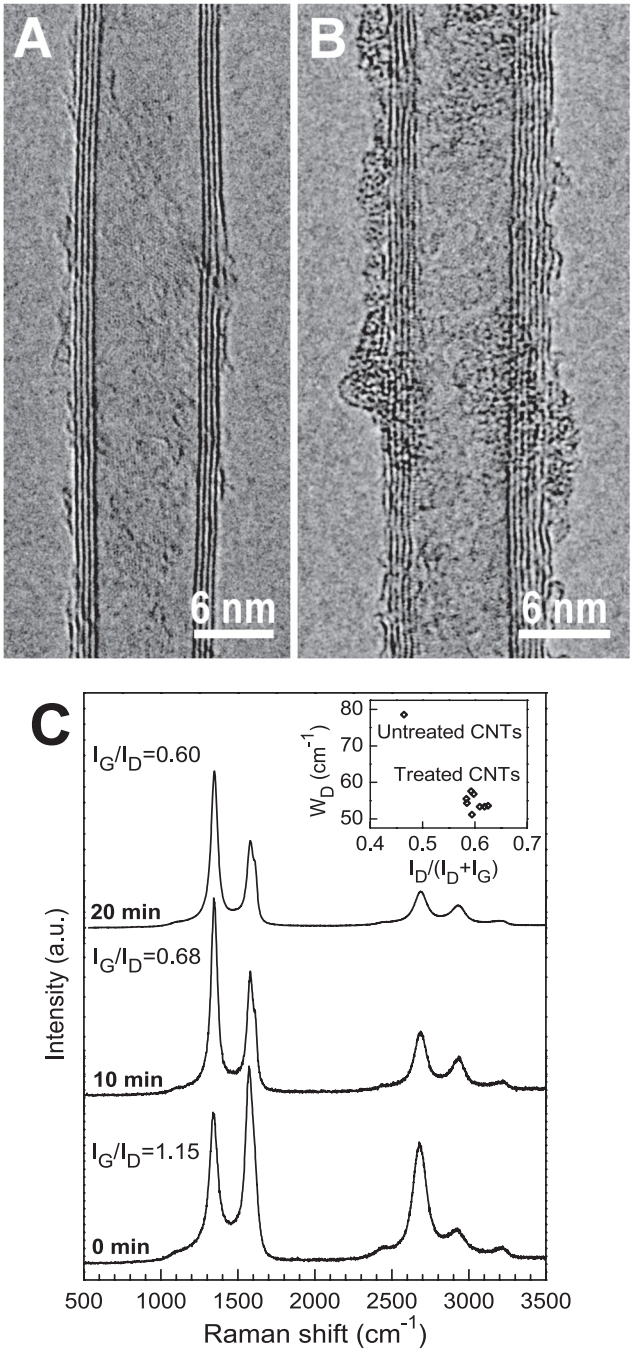

Figure 1. TEM images of CNTs before (A) and after (B) 10 minutes of exposure to the NH_3/He plasma. The increased surface roughness in (B) is related to the decrease in inter-nanotube order as a result of plasma treatment. C) Intensity normalized Raman spectra (λ = 514 nm) of plasma generated CN_x (p-CN_x) for different plasma exposure times. Inset: D-band FWHM versus Raman disorder parameter for CNTs before and after plasma treatment.

first-order Raman modes located at ~1580 cm^{-1} (E_{2g} or G-band) for a 514 nm laser wavelength[34] correlate with the amount of defects existing within the nanotube shells.[35] The evolution of the integrated peak intensity ratio, I_D/I_G, from 0.87 for pristine CNTs to 1.46 after 10 minutes of plasma treatment indicates an increase of the degree of disorder in the nanotubes and a decrease in the size of graphitic domains.[34,35]

The FWHM of the D-band (W_D) is plotted as function of the Raman-derived degree of disorder, $I_D/(I_D + I_G)$,[36] in the inset of Figure 1C, which shows that these parameters for plasma treated MWNTs are located in a well-defined coordinates region that is well separated from the coordinates for the pristine MWNTs. On the other hand, the surface order of the plasma exposed MWNTs (or parameter for graphitization) reflected by W_G[37] decreased by only about 5 cm^{-1} upon plasma treatment, which lead to a fairly constant W_G/W_D ratio of between 1.23 and 1.29 for plasma doping times between 2.5 and 20 minutes; while undoped CNTs exhibit W_G/W_D values of 0.94. Although this loss of MWNT sidewall order provides indirect evidence suggesting doping, since generated defects are expected from incorporating foreign atoms, no large shifts of the D- and G-bands were observed upon plasma doping.[38,39] However, small peak shifts towards higher frequencies, apparently uncorrelated to the plasma treatment time, were found for both D (4 ± 1 cm^{-1}) and G (8 ± 2 cm^{-1}) bands. The behavior observed in these Raman spectra is consistent with plasma processes that promote structural defects and lead to low dopant concentrations, but do not substantially affect the frequencies of D and G bands.

Evidence for nitrogen doping in the NH_3/He plasma treated CNTs was then investigated by X-Ray photoelectron spectroscopy (XPS), since its sensitivity range is tenths of atomic percent[40] and this method can provide information about the chemical states of individual atoms. XPS spectra were recorded using an Al monochromatic source (1486.6 eV and 350.0 W) with constant pass energy of 29 eV. For analysis purposes the C 1s signal was assigned to a binding energy (BE) of 284.6 eV.[41,42] In addition to the expected C 1s peak, full-range survey scans (Figure S1 in the Supporting Information) on plasma-treated CNT sheets revealed another main peak at 399 eV, corresponding to the BE of N 1s electrons, which was not observed in untreated CNTs. Evolution in intensity of the O 1s main peak signal (~532.4 eV) was also found for the NH_3/He plasma treated CNTs. The presence of this peak in XPS is due to adsorbed oxygen contaminants on the rough surface of plasma-treated CNTs[43] and to the native SiO_2 layer on the Si wafer used as substrate for the XPS analysis. Since the N-doping in these plasma-treated CNTs has now been established, we will hereafter legitimately refer to them as plasma doped CN_x, or p-CN_x.

Detailed XPS spectra for the C 1s and N 1s electronic states were acquired for p-CN_x produced using different plasma exposure times. The BE of N 1s spectra were calibrated versus the C 1s peak value,[44] and the nitrogen atomic ratio (N/C), at.%, was calculated using the areas of the N 1s and C 1s signals weighted by their individual sensitivity factors. Peaks asymmetries indicate the existence of more than one chemical species,[31] which can be identified by deconvoluting the peak into multiple Gaussian curves.[39] Shirley background was substracted and the simulated FWHM was kept constant for each signal in a given spectra. The data in **Figure 2** shows that the N/C ratio consistently increases with increasing plasma exposure time, providing: 1.2, 1.8, 2.1, 2.6, and 4.5 at.% N for 5, 7.5, 10, 15, and 20 minutes of plasma exposure, respectively. Deconvolution of these N 1s main peaks allowed us to

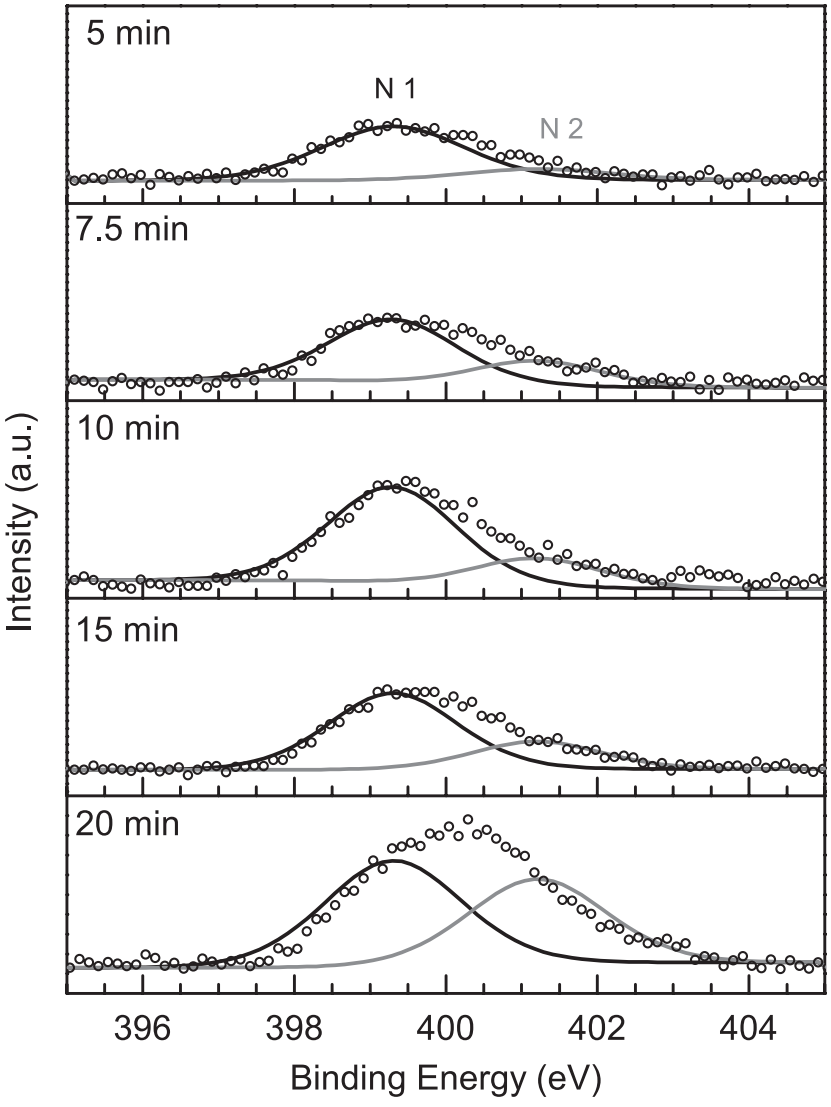

Figure 2. Deconvolution analysis for the N 1s peak in the XPS spectra of p-CN_x as a function of plasma doping time. N1 (black) and N2 (gray) curves stand for pyridinic N (pyr-N), and N substitutionally bound to three carbon atoms (q-N), respectively.

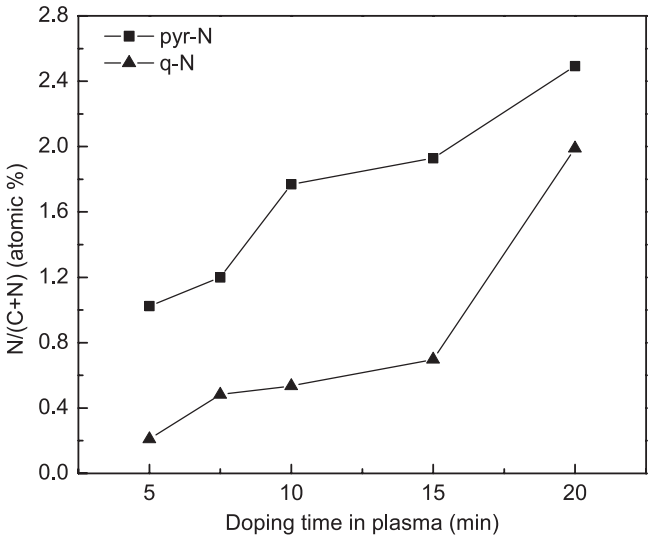

Figure 3. Atomic concentration of the main chemical species of nitrogen identified in p-CN_x as function of doping time, where N/(C+N) is an abbreviated designation for the atomic concentration of a particular N species (pyr-N or q-N) divided by the total atomic concentrations of N and C.

identify chemically different types of N within the p-CN_x as: 1) pyridinic nitrogen, pyr-N, at a BE of 398.4–399.0 eV (where the N-atom contributes one p-electron to the π system[44,45]); 2) N substitutionally bonded to three neighboring carbon atoms in a sp^2 hexagonal graphene network[32] or quaternary N, q-N (BE of 399.9–401.9 eV).[45] This latter BE region overlaps with that for NH_2 groups (BE of 400.23–400.44 eV).[41] Relative concentrations of these nitrogen species, $N_i/(N_T+C)$, as function of doping time are summarized in **Figure 3**, where N_i is the atomic concentration for a particular specie and N_T+C is the total atomic concentration of N and C.

Having now demonstrated the feasibility of using an NH_3/He plasma method to dope CNTs with nitrogen, we next assessed the possibility of practical applications by determining the catalytic activity of the resulting CN_x, the mechanical strength of yarns containing CN_x, and other relevant properties, like surface energy and gravimetric capacitance.

Since the presence of nitrogen doping alters nanotube roughness (Figures 1A,B) and likely changes surface energies, we examined the effect of 10 minutes of plasma doping on nanotube sheet surface tension, which is an important factor for electrochemical applications. **Figures 4**A,B reveal a slightly higher contact angle for a water droplet supported by a free standing p-CN_x sheet (Figure 4B) than for a sheet of pristine MWNTs. This indicates that these plasma treated CNTs become slightly more hydrophilic when compared to the undoped material (Figure 4A).

We next describe the fabrication of p-CN_x yarn from p-CN_x sheet obtained after doping a stack of 4 MWNT sheets. After 10 minutes of plasma treatment, a 4-mm-wide free-standing aerogel sheet of p-CN_x sheets (having an areal density of only ~5 $\mu g \cdot cm^{-2}$) was still sufficiently strong to support a metal bar weighing 23 mg. This metal bar (driven by a rotating magnetic field from a standard magnetic stirrer plate) was used to twist the aerogel sheet into a five-centimeter-long p-CN_x yarn (Figure 4C). Such p-CN_x yarns (obtained by dry-state insertion of 1350 turns $\cdot m^{-1}$ twist) have a SEM-observed topology (Figure 4E), that is indistinguishable from that of similarly prepared yarns of undoped MWNTs.

These p-CN_x yarns can be easily sewn into textiles (**Figure 5**C), woven, and knotted. The measured tensile specific strength (i.e., strength normalized by linear mass density) for p-CN_x yarns is 451 ± 61 MPa $\cdot cm^3 \cdot g^{-1}$, which is 68% of the specific tensile strength obtained for similarly prepared single-ply undoped MWNT yarn, 667 ± 53 MPa $\cdot cm^3 \cdot g^{-1}$. However, the p-CN_x yarns produced in this work are much stronger than previously showed yarns prepared by biscrolling 70 wt.% s-CN_x powder in a MWNT host, which have a specific strength of 138 MPa $\cdot cm^3 \cdot g^{-1}$.[21]

Liquid-driven densification that occurs during the preparation of biscrolled yarns containing s-CN_x powder increases the basic structural differences between the yarns and p-CN_x yarns

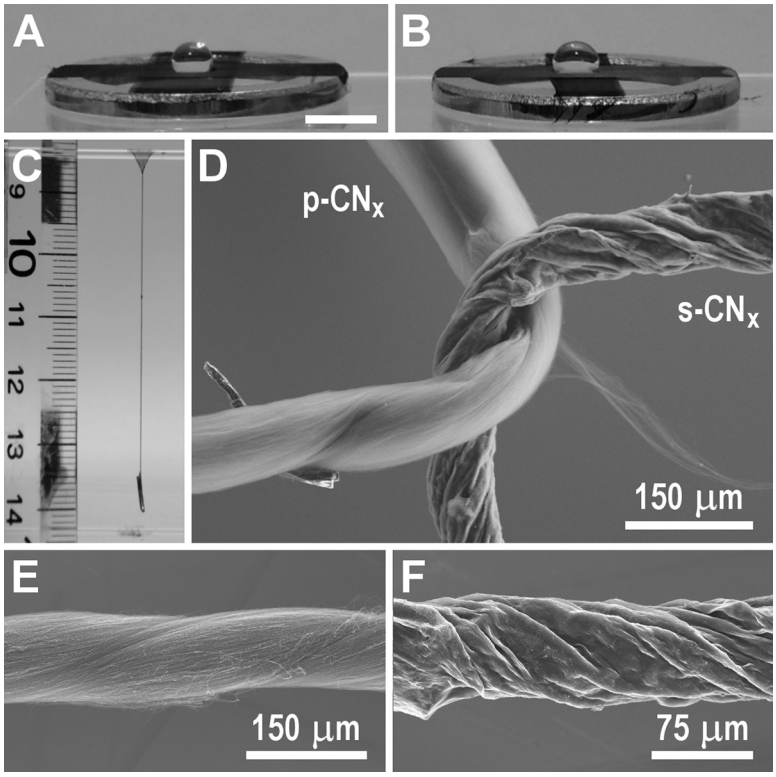

Figure 4. Droplets of water on free-standing CNT sheets before (A) and after (B) NH_3/He plasma treatment for 10 minutes to produce a CN_x sheet. C) A 5 cm long CN_x yarn obtained by twist insertion into a plasma-treated free-standing sheet, showing at its lower end the magnetic bar used to insert twist. D) A SEM image of a p-CN_x dry-twisted yarn (left) linked to a CN_x-containing biscrolled yarn that was twist spun in liquid (acetone) (right). E,F) Higher magnification SEM images of the sides of the above p-CN_x and s-CN_x-containing biscrolled yarn, respectively. The barber pole type structure, evident in E, is consequence of the dual-Archimedean scroll[21] that results from twist insertion in a nanotube sheet attached between two rigid supports. Unless otherwise specified, here and elsewhere, plasma treatment time of the sheet precursor for the dry-spun CN_x yarns was 10 minutes.

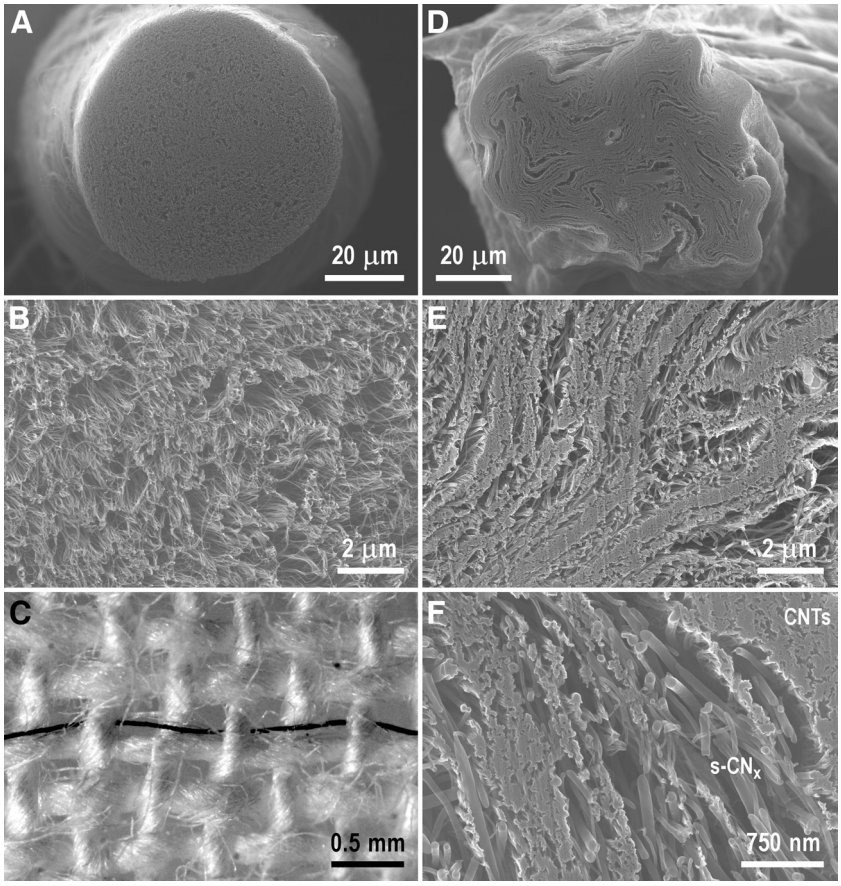

Figure 5. Cross-sectional SEM images prepared by ion milling of (A,B) a p-CN_x-yarn obtained by twist insertion in the dry-state and (D,F) a biscrolled s-CN_x-containing yarn obtained by twist insertion in the liquid state. Regions with higher nanotube density in (E,F) correspond to the undoped MWNTs in the host sheet, while lower density regions correspond to the guest s-CN_x powder. C) Optical picture of a CN_x-yarn (black) sewn into a cotton fabric. This yarn was made by dry-state twist insertion into a p-CN_x sheet doped for 12.5 minutes in a NH_3/He plasma.

obtained by dry-state twist insertion (Figures 4D–F). SEM images of the cross-sections of these CN_x-yarns (prepared by Ga-ion beam cutting and milling using a focused ion beam) (Figure 5A) show that CN_x yarns prepared by dry-state twist insertion of plasma-treated MWNT sheets have round cross sections and more homogeneously distributed nanotube density than the liquid processed biscrolled yarns containing s-CN_x powder.

Figure 5A, B shows a 67 μm diameter p-CN_x yarn (inserted twist of 3250 turns·m^{-1}) with a density of ~0.2 g·cm^{-3}. This density was estimated from the theoretically predicted nanotube bundle density of ~1.39 g·cm^{-3}[21] and the measured yarn linear density of 0.5 mg·m^{-1} (equivalent to a nanotube areal density of 10^3 CN_x·μm^{-2}), which provides a void fraction (F_{void}) of roughly 0.89. Yarn density can be tuned by controlling the amount of inserted twist and by following dry-state twist insertion with surface-tension-based liquid-produced densification.

Biscrolled yarns of s-CN_x, on the other hand, have irregular cross-sections (Figure 5D) and alternating zones of undoped and N-doped nanotubes within a yarn cross-section, which have different densities (Figures 5E,F). The existence of a complex scroll structure formed by galleries of densified sheets of ~9 nm diameter undoped nanotubes holding ~50 nm diameter s-CN_x nanotubes is result of non-ideal dual-Archimedean scrolling.[21] Liquid-based densification associated with twist insertion in a liquid is capable of achieving the highest degree of compaction (ca. 0.8 g·cm^{-3},[21] equivalent to a F_{void} of 0.42 and ~5 × 10^3 CNT·μm^{-2}) for the MWNT sheet that acts as host in the biscrolled yarn (Figure 5F). Since the s-CN_x nanotube powder is largely unaligned, the volumetric density in the guest region of the biscrolled yarn is much lower (~0.14 g·cm^{-3}).

As shown by Lima et al.,[21] s-CN_x/CNT yarns (90 wt.% s-CN_x guest in a MWNT host) inherit the catalytic properties of the s-CN_x for catalyzing oxygen reduction in an acidic electrolyte medium, by shifting the onset potential +0.28 V with respect to that for undoped MWNTs.[19] These results are in good agreement with those of various authors[17–20] who have been extensively studying the electrochemical catalytic activity of N-doped CNTs, and attributed it to the extent of nitrogen doping within the CN_x (and more importantly to the ratio of pyridinic to quaternary functionalities).

Based on these literature results,[17–20] incorporation of nitrogen is not per se sufficient to assert catalytic behavior for the p-CN_x yarns prepared by the present plasma treatment process. Therefore, we conducted cyclic voltammetry (CV) on p-CN_x yarns using a similar setup to that used for measuring the catalytic activity of s-CN_x powder in biscrolled yarns (using Pt mesh as counter electrode and Ag/AgCl/3 M NaCl as reference electrode in an oxygen saturated 0.5 M H_2SO_4 solution).[21] The CV curves in **Figure 6**A show that the onset potential for oxygen reduction shifts towards positive values as a function of plasma doping time for the MWNTs, reaching a maximum of +0.24 V after 10 minutes of plasma treatment, which is only 0.04 V lower than obtained for presently tested biscrolled yarns containing s-CN_x. Catalytic activity for these p-CN_x yarns is not lost after 200 cycles (Figure S2 in the Supporting Information) indicating that the N-doping obtained is stable in the electrochemical system described above. Plasma exposure times longer than 10 minutes decreased the onset potential for ORR by p-CN_x yarns; the longest treatment time (20 minutes) exhibited an onset potential of 0.12 V, which is close to the exhibited by undoped MWNT yarns.

This decrease in onset potential for oxygen reduction for plasma treatment times above 10 minutes contrasts with the observation that the atomic fraction of total N concentration increases nearly monotonically with plasma treatment time, as shown in Figures 2 and 3. However, the XPS measurements indicate that the ratio of atomic percentages of pyridinic to substitutional N reached a maximum of 3.3 (Figure 3) for MWNTs exposed to 10 minutes of plasma treatment. Longer plasma treatment times increased the total amount of N by adding mostly q-N species, stretching the ratio between the atomic

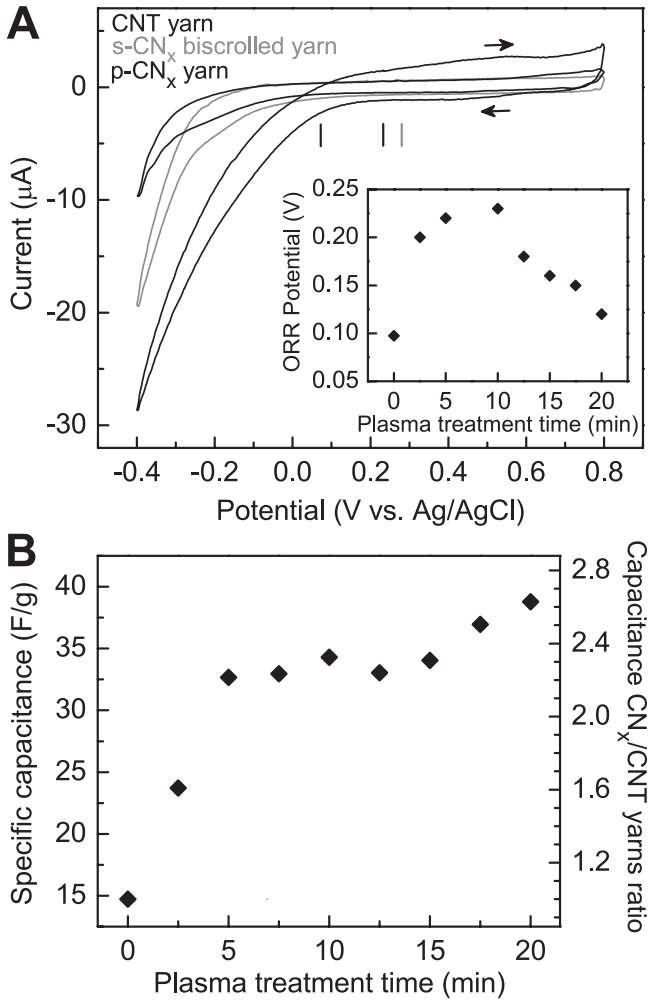

Figure 6. Electrochemical characterization of p-CN_x yarns. A) Cyclic voltammetry curves at 5 $mV \cdot s^{-1}$ for an undoped dry-twisted MWNT yarn (black); a biscrolled yarn containing 90 wt.% s-CN_x guest in a MWNT host (light gray) and a p-CN_x yarn (dark gray). The inset in (A) is the observed shift in onset potential (denoted by the vertical lines) for the ORR as a function of NH_3/He plasma treatment time. B) The dependence of the specific capacitance of p-CN_x yarns as function of plasma treatment time. Capacitance values were obtained by slope analysis of the curves *I* vs. scan rate exhibited by the yarns for potentials in the range of 0.2–0.6 V (*vs.* Ag/AgCl 3 M NaCl) using a 0.5 M H_2SO_4 solution as electrolyte.

percentages of pyr-N to q-N. Thus, it appears that increasing concentrations of non-pyridinic nitrogen can degrade catalytic activity that is enhanced by pyridinic nitrogen.

Importantly, the specific capacitance of p-CN_x yarns (shown in Figure 6B) dramatically increased with the plasma treatment time, from 14.7 $F \cdot g^{-1}$ for undoped CNT yarns to 38.8 $F \cdot g^{-1}$ for yarns made of 20 minute plasma treated MWNTs. This increase in capacitance is likely caused by an increase of nanotube surface area as a result of nanotube etching during plasma treatment.

In order to better resolve the convoluted peaks corresponding to different chemical species in the N 1s XPS spectra shown in Figure 2, thermal annealing treatments were performed on the p-CN_x samples, which were inspired by the results of Xu et al.[32] While the N 1s peak splitting was not readily observed, probably due to relatively low annealing temperatures, consistent reduction of N/C abundances ratio was found for p-CN_x annealed at temperatures ranging from 200 °C to 500 °C (see Figure S3 in the Supporting Information). N/C ratios decreased to below 1 at.% for all p-CN_x annealed at 500 °C and the onset potential for oxygen reduction decreased to ~0.11 V independent of the plasma doping time, thus indicating a loss of the previously gained catalytic activity due to nitrogen doping.

3. Conclusions

We report a simple process for the conversion of highly oriented, forest-drawn MWNT sheets into weavable, sewable, and knottable N-doped nanotube yarns that have high strength, catalytic activity for oxygen reduction, and enhanced gravimetric capacitance. Nitrogen doping was accomplished by exposure of the as-drawn, self-supported MWNT sheets to a NH_3/He plasma. For N/C ratios as high as 2.6 at.%, this procedure enabled control of N doping within the nanotubes without causing dramatic loss of sheet or yarn strength. XPS measurements show the evolution of dopant species as a function of plasma treatment time and demonstrate that thermal anneal after doping at as low as 200 °C can dramatically reduce total nitrogen concentration and essentially eliminate catalytic performance enhancement. This catalytic activity for oxygen reduction was maximized for a pyridinic N concentration of ~1.8 at.% and high values of the concentration ratio of pyridinic to non-pyridinic N species, which was obtained for 10 minutes of plasma treatment. Although longer plasma treatment times increased the total concentration of nitrogen, catalytic performance sharply degraded, likely because the increasing concentrations of non-pyridinic species. The p-CN_x yarns produced by the plasma doping method has very high specific strength (451 ± 61 $MPa \cdot cm^3 \cdot g^{-1}$) and a gravimetric capacitance (up to 39 $F \cdot g^{-1}$) that was 2.6 times higher than for similarly prepared undoped MWNT. Performance comparisons with biscrolled yarns containing powder of N-doped nanotubes showed a slightly higher potential for oxygen reduction for the biscrolled yarn and a much higher strength for the N-doped yarn made by plasma treatment and major structural differences in the two types of catalytic yarns. Upon further enhancing catalytic performance, such as by optimizing the choice of plasma gases, the strong twist-spun N-doped yarns made by the plasma process might find application as flexible woven textiles for fuel cells and for metal-air batteries.

4. Experimental Section

Nanotube Synthesis: The two different types of nanotubes used as starting material in this work are: i) undoped, spinnable MWNT forests synthesized by a seeded catalyst thermal chemical vapor deposition (CVD) (by pyrolysing acetylene in an Ar/H_2 (15:2 v:v) atmosphere at 700 °C),[21] and ii) N-doped MWNTs (s-CN_x) that were doped during synthesis using floating-catalyst CVD method (by pyrolysing a 2.5 wt.% mixture of ferrocene, η^5-$Fe(C_5H_5)_2$ and benzylamine, $C_7H_7NH_2$ in an Ar atmosphere at 860 °C).[22]

General Characterization Methods: Raman and XPS measurements were performed on stacks of several layers (typically 20) of undensified p-CN_x or MWNT sheets placed on the surface of clean Si wafers (without stripping their native oxide layer).

Specific yarn tensile strength was obtained by using a 5 mm gauge length and an elongation rate of 0.5 mm·min^{-1} in a FAVIMAT tensile tester. Specific strengths are reported to avoid errors due to the measurement of cross-sectional area. They were computed by dividing the rupture force (F) between the linear mass density of the yarn (ρ_l, mass divided per length) or F/ρ_l.

Yarn Cross-sections Preparation and Imaging: p-CN_x and s-CN_x biscrolled yarns were cut across their diameters by a FIB FEI Nova 200 operated at 30 kV and 7 nA of beam current. After cut, the cross sections were ion-polished over several micrometers along the yarn length by ion beam currents ranging from 7.0 nA to 0.5 nA. Once the cleaning procedure was finished, the yarns were transferred to 90° SEM holders (Ted Pella, Inc.) with their cross-sections facing the incoming electron beam (SEM Zeiss Supra 40) in order to perform detailed microscopic analysis.

Electrochemical Studies: s-CN_x biscrolled yarns used as working electrodes were prepared by twisting in liquid a stack of a MWNT sheet with deposited s-CN_x by wet filtration as described previousy in Lima et al.[21] Undoped MWNT yarns with similar linear densities to s-CN_x biscrolled yarns (~15 μg·cm^{-1}) were achieved by stacking 8 layers of free standing sheets and inserting twist in air; p-CN_x yarns were produced in a similar way. For electrochemical measurements, yarns were supported at opposite ends to enable their submersion in the electrolyte (0.5 M H_2SO_4 aqueous solution) saturated with O_2 by air bubbling.

Supporting Information

Supporting Information is available from the Wiley Online Library or from the author.

Acknowledgements

This work was supported by the Air Force Office of Scientific Research MURI grant on Tunable 3D Nanotube Architectures, Robert A. Welch Foundation Grant AT-0029 and CONACYT-México-UTD (for the Ph.D. scholarship of X.L.). M.T. acknowledges support from the Research Center for Exotic NanoCarbons, Japan regional Innovation Strategy Program by the Excellence, JST.

Received: August 25, 2011
Revised: October 20, 2011
Published online: December 19, 2011

[1] M. M. J. Treacy, T. W. Ebbesen, J. M. Gibson, *Nature* **1996**, *381*, 678.
[2] A. Krishnan, E. Dujardin, T. W. Ebbesen, P. N. Yianilos, M. M. J. Treacy, *Phys. Rev. B* **1998**, *58*, 14013.
[3] S. Akita, H. Nishijima, Y. Nakayama, F. Tokumasu, K. Takeyasu, *J. Phys. D: App. Phys.* **1999**, *32*, 1044.
[4] Z. Spitalsky, D. Tasis, K. Papagelis, C. Galiotis, *Prog. Polym. Sci.* **2010**, *35*, 357.
[5] K. Jiang, Q. Li, S. Fan, *Nature* **2002**, *419*, 801.
[6] M. Zhang, K. R. Atkinson, R. H. Baughman, *Science* **2004**, *306*, 1358.
[7] A. A. Zakhidov, R. Nanjundaswamy, A. N. Obraztsov, M. Zhang, S. Fang, V. I. Klesh, R. H. Baughman, A. A. Zakhidov, *Appl. Phys. A: Mater. Sci. Process.* **2007**, *88*, 593.
[8] K. R. Atkinson, S. C. Hawkins, C. Huynh, C. Skourtis, J. Dai, M. Zhang, S. L. Fang, A. A. Zakhidov, S. B. Lee, A. E. Aliev, C. D. Williams, R. H. Baughman, *Phys. B: Condensed Matter* **2007**, *394*, 339.
[9] C. D. Williams, R. Ovalle Robles, M. Zhang, S. Li, R. H. Baughman, A. A. Zakhidov, *Appl. Phys. Lett.* **2008**, *93*, 183506.
[10] Y. L. Li, I. A. Kinloch, A. H. Windle, *Science* **2004**, *304*, 276.
[11] D. S. Lashmore, R. Braden, A. J. Hart, J. Welch, *US Patent 2009029341*, **2009**.
[12] Q. Li, X. Zhang, R. F. DePaula, L. Zheng, Y. Zhao, L. Stan, T. G. Holesinger, P. N. Arendt, D. E. Peterson, Y. T. Zhu, *Adv. Mater.* **2006**, *18*, 3160.
[13] K. Liu, Y. H. Sun, L. Chen, C. Feng, X. F. Feng, K. L. Jiang, Y. G. Zhao, S. S. Fan, *Nano Lett.* **2008**, *8*, 700.
[14] Y. Nakayama, *Jpn. J. Appl. Phys., Part 2* **2008**, *47*, 8149.
[15] X. Lepró, M. D. Lima, R. H. Baughman, *Carbon* **2010**, *48*, 3621.
[16] C. P. Huynh, S. C. Hawkins, *Carbon* **2010**, *48*, 1105.
[17] S. Maldonado, K. J. Stevenson, *J. Phys. Chem. B* **2005**, *109*, 4707.
[18] Y. Shao, J. Sui, G. Yin, Y. Gao, *Appl. Catal. B* **2008**, *79*, 89.
[19] S. Kundu, T. C. Nagaiah, W. Xia, Y. Wang, S. V. Dommele, J. H. Bitter, M. Santa, G. Grundmeier, M. Bron, W. Schuhmann, M. Muhler, *J. Phys. Chem. C* **2009**, *113*, 14302.
[20] K. Gong, F. Du, Z. Xia, M. Durstock, L. Dai, *Science* **2009**, *323*, 760.
[21] M. D. Lima, S. Fang, X. Lepró, C. Lewis, R. Ovalle Robles, J. Carretero González, E. Castillo Martínez, M. Kozlov, J. Oh, N. Rawat, C. S. Haines, M. H. Haque, V. Aare, S. Stoughton, A. A. Zakhidov, R. H. Baughman, *Science* **2011**, *331*, 51.
[22] M. Terrones, R. Kamalakaran, T. Seeger, M. Rühle, *Chem. Commun.* **2000**, 2335.
[23] M. Terrones, H. Terrones, N. Grobert, W. K. Hsu, Y. Q. Zhu, J. P. Hare, H. W. Kroto, D. R. M. Walton, P. Kohler-Redlich, M. Ruhle, J. P. Zhang, A. K. Cheetham, *Appl. Phys. Lett.* **1999**, *75*, 3932.
[24] M. Terrones, N. Grobert, J. Olivares, J. P. Zhang, H. Terrones, K. Kordatos, W. K. Hsu, J. P. Hare, P. D. Townsend, K. Prassides, A. K. Cheetham, H. W. Kroto, D. R. M. Walton, *Nature* **1997**, *388*, 52.
[25] R. Sen, B. Satishkumar, S. Govindaraj, K. Harikumar, M. Renganathan, C. Rao, *J. Mater. Chem.* **1997**, *7*, 2335.
[26] T.-Y. Kim, K.-R. Lee, K. Y. Eun, K.-H. Oh, *Chem. Phys. Lett.* **2003**, *372*, 603.
[27] Y. T. Lee, N. S. Kim, S. Y. Bae, J. Park, S.-C. Yu, H. Ryu, H. J. Lee, *J. Phys. Chem. B* **2003**, *107*, 12958.
[28] J. W. Jang, C. E. Lee, S. C. Lyu, T. J. Lee, C. J. Lee, *Appl. Phys. Lett.* **2004**, *84*, 2877.
[29] D. Golberg, Y. Bando, W. Han, K. Kurashima, T. Sato, *Chem. Phys. Lett.* **1999**, *308*, 337.
[30] W. Han, Y. Bando, K. Kurashima, T. Sato, *Chem. Phys. Lett.* **1999**, *299*, 368.
[31] C. Morant, J. Andrey, P. Prieto, D. Mendiola, J. M. Sanz, E. Elizalde, *Phys. Status Solidi A* **2006**, *203*, 1069.
[32] F. Xu, M. Minniti, P. Barone, A. Sindona, A. Bonanno, A. Oliva, *Carbon* **2008**, *46*, 1489.
[33] L. H. Chan, K. H. Hong, D. Q. Xiao, T. C. Lin, S. H. Lai, W. J. Hsieh, H. C. Shih, *Phys. Rev. B* **2004**, *70*, 125408.
[34] Y. Wang, D. C. Alsmeyer, R. L. McCreery, *Chem. Mater.* **1990**, *2*, 557.
[35] Z. Xu, C. Min, L. Chen, L. Liu, G. Chen, N. Wu, *J. Appl. Phys.* **2011**, *109*, 054303.
[36] A. Cuesta, P. Dhamelincourt, J. Laureyns, A. Martínez-Alonso, J. M. D. Tascón, *Carbon* **1994**, *32*, 1523.
[37] A. Yoshida, Y. Kaburagi, Y. Hishiyama, *Carbon* **2006**, *44*, 2333.
[38] Q.-H. Yang, P.-X. Hou, M. Unno, S. Yamauchi, R. Saito, T. Kyotani, *Nano Lett.* **2005**, *5*, 2465.
[39] K. Ghosh, M. Kumar, T. Maruyama, Y. Ando, *Carbon* **2010**, *48*, 191.
[40] L. C. Feldman, J. W. Mayer, *Fundamentals of Surface and Thin Film Analysis*, North-Holland, New York **1986**.
[41] T. I. T. Okpalugo, P. Papakonstantinou, H. Murphy, J. McLaughlin, N. M. D. Brown, *Carbon* **2005**, *43*, 153.
[42] M. T. Martínez, M. A. Callejas, A. M. Benito, M. Cochet, T. Seeger, A. Ansón, J. Schreiber, C. Gordon, C. Marhic, O. Chauvet, J. L. G. Fierro, W. K. Maser, *Carbon* **2003**, *41*, 2247.
[43] H. C. Choi, S. Y. Bae, W.-S. Jang, J. Park, H. J. Song, H.-J. Shin, H. Jung, J.-P. Ahn, *J. Phys. Chem. B* **2005**, *109*, 1683.
[44] R. Arrigo, M. Hävecker, R. Schlögl, D. S. Su, *Chem. Commun.* **2008**, 4891.
[45] F. Kapteijn, J. A. Moulijn, S. Matzner, H. P. Boehm, *Carbon* **1999**, *37*, 1143.